Polarimetric Change Analysis in Forest using PolInSAR Ground and Volume separation techniques

Alberto Alonso-Gonzalez[a] and Konstantinos P. Papathanassiou[a]
[a]German Aerospace Center (DLR), Muenchner Str. 20, 82234 Oberpfaffenhofen-Wessling, Germany

Abstract

This work employs a Polarimetric SAR Interferometry (PolInSAR) two-layer model in order to separate the polarimetric response from ground and volume contributions in vegetated scenarios. The full rank covariance matrix for the ground and volume components may be extracted. The polarimetric properties of the extracted components will be evaluated under different acquisition conditions, in order to better understand the potentials of the PolInSAR separation technique for bio/geo-physical parameters extraction.

1 Introduction

SAR Polarimetry (PolSAR) allows to discriminate different geometric and dielectric properties of scatterers within the resolution cell. Several polarimetric ground and volume models have been employed to extract bio/geophysical properties of the scene. However, in a real scenario, the radar response of ground and volume contributions are mixed together over vegetated areas. On the other hand SAR Interferometry, by exploiting acquisitions with different baselines, has sensitivity to the vertical distribution of scatterers. This work combines SAR Polarimetry and Interferometry (PolInSAR) in order to separate ground and volume components assuming a two-layer model.

2 The PolInSAR two-layer model

PolInSAR sensors measure the fully polarimetric response of the target at N different baselines. Therefore, the Multipolarization Multibaseline coherency matrix $\mathbf{T}_N$ may be expressed as

$$\mathbf{T}_N = \langle \mathbf{k}\mathbf{k}^H \rangle = \begin{pmatrix} \mathbf{T}_{11} & \mathbf{\Omega}_{12} & \cdots & \mathbf{\Omega}_{1N} \\ \mathbf{\Omega}_{12}^H & \mathbf{T}_{22} & \cdots & \mathbf{\Omega}_{2N} \\ \vdots & \vdots & \ddots & \vdots \\ \mathbf{\Omega}_{1N}^H & \mathbf{\Omega}_{2N}^H & \cdots & \mathbf{T}_{NN} \end{pmatrix} \tag{1}$$

$$\mathbf{k} = \left[\mathbf{k}_1^T \mathbf{k}_2^T \cdots \mathbf{k}_N^T \right]^T \tag{2}$$

$$\mathbf{k}_i = \frac{1}{\sqrt{2}} \left[\; S_{hh}^i + S_{vv}^i, \quad S_{hh}^i - S_{vv}^i, \quad S_{hv}^i + S_{vh}^i \; \right]^T. \tag{3}$$

where $\mathbf{T}_{ii}$ represent the polarimetric coherency matrix at baseline i and $\mathbf{\Omega}_{ij}$ represents the PolInSAR matrix between baselines i and j.

Traditionally, in the two layer models the scattering is decomposed into two main physical components: the soil, considered as an impenetrable surface, and the vegetation on top of it, represented by a volume of small scatterers. These models have been also employed for interferometry as, for instance, the Random Volume Over Ground (RVOG) [5] or the interferometric water cloud model (IWM) [4].

In the two layer model the interferometric coherence γ_{ij} between acquisition i and j for a particular polarization state $\mathbf{w}$ may be expressed as [5]

$$\gamma_{ij}(\mathbf{w}) = \frac{\mathbf{w}^H \mathbf{\Omega}_{ij} \mathbf{w}}{\sqrt{\mathbf{w}^H \mathbf{T}_{ii} \mathbf{w} \cdot \mathbf{w}^H \mathbf{T}_{jj} \mathbf{w}}} = \frac{\gamma_{ij}^v + \gamma_{ij}^g \mu(\mathbf{w})}{1 + \mu(\mathbf{w})} \tag{4}$$

where γ_{ij}^g and γ_{ij}^v represent the interferometric coherence for the ground and volume layers, respectively, defined as

$$\gamma_{ij}^l = \frac{\int F^l(z) e^{j k_{z_{ij}} z} \, dz}{\int F^l(z) \, dz}, \tag{5}$$

with $l \in (g, v)$, $k_{z_{ij}}$ is the vertical wavenumber between acquisition i and j, and $\mu(w)$ represents the ground to volume power ratio for the polarization state $\mathbf{w}$

$$\mu(\mathbf{w}) = \frac{\mathbf{w}^H \mathbf{T}_g \mathbf{w}}{\mathbf{w}^H \mathbf{T}_v \mathbf{w}}. \tag{6}$$

As mentioned in [5], under these assumptions the coherence region for each baseline $\gamma_{ij}(\mathbf{w})$ is following a segment of the line defined by the two layers coherences γ_{ij}^g and γ_{ij}^v controlled by the ground to volume ratio $\mu(\mathbf{w})$. Different two layer models differ only in the interpretation of these layers and/or their vertical characteristics $F^l(z)$ definition.

3 Ground and Volume Response Separation

This two layer model formulation is convenient since (4) indirectly separates the polarimetric and interferometric components into the $\mu(\mathbf{w})$ and γ_{ij}^g, γ_{ij}^v factors, respectively. The assumption behind this fact is that the scene and the

vertical distribution of scattering are not changing between baselines and polarizations. This allows one to define the different coherence $\mathbf{T}_{ii}$ and PolInSAR $\mathbf{\Omega}_{ij}$ matrices in (1) as already noted in [6] [7]

$$\mathbf{T}_{ii} = \mathbf{T}_g + \mathbf{T}_v \tag{7}$$

$$\mathbf{\Omega}_{ij} = \gamma_{ij}^g \mathbf{T}_g + \gamma_{ij}^v \mathbf{T}_v \tag{8}$$

For a more concise multibaseline notation, the representation of the two layer models covariance matrix $\mathbf{T}_N$ defined in (1) may be expressed by a Sum of Kronecker Products (SKP), as described in [8]

$$\mathbf{T}_N = \mathbf{R}_g \otimes \mathbf{T}_g + \mathbf{R}_v \otimes \mathbf{T}_v \tag{9}$$

where $\mathbf{R}_g$ and $\mathbf{R}_v$ represent the $N \times N$ structure matrices and $\mathbf{T}_g$ and $\mathbf{T}_v$ the 3×3 coherency matrices of the ground and volume, respectively.
Instead of working directly over the $\mathbf{\Omega}_{ij}$ matrices a polarimetric pre-whitening filter may be applied. This filter simplifies the formulation as the interferometric coherences may be obtained as the numerical range of the $\mathbf{\Pi}_{ij}$ matrices [7]

$$\mathbf{\Pi}_{ij} = \mathbf{T}_{ii}^{\frac{-1}{2}} \mathbf{\Omega}_{ij} \mathbf{T}_{jj}^{\frac{-1}{2}} = \gamma_{ij}^g \mathbf{T}_{gw} + \gamma_{ij}^v \mathbf{T}_{vw} \tag{10}$$

where $\mathbf{T}_{gw}$ and $\mathbf{T}_{vw}$ correspond to the whitened ground and volume coherency matrices, having

$$\mathbf{I} = \mathbf{T}_{gw} + \mathbf{T}_{vw}. \tag{11}$$

From (10) and (11), the whitened ground and volume coherency matrices may be extracted for every i, j acquisition combination by fixing the γ_{ij}^g and γ_{ij}^v as

$$\hat{\mathbf{T}}_{vw}^{(ij)} = H\left(\frac{\mathbf{\Pi}_{ij} - \gamma_{ij}^g \mathbf{I}}{\gamma_{ij}^v - \gamma_{ij}^g}\right) \tag{12}$$

$$\hat{\mathbf{T}}_{gw}^{(ij)} = H\left(\frac{\mathbf{\Pi}_{ij} - \gamma_{ij}^v \mathbf{I}}{\gamma_{ij}^g - \gamma_{ij}^v}\right) \tag{13}$$

where $H(\mathbf{A})$ denotes the Hermitian part of matrix $\mathbf{A}$, defined as $H(\mathbf{A}) = (\mathbf{A} + \mathbf{A}^H)/2$.
In a multibaseline scenario, $\hat{\mathbf{T}}_{gw}^{(ij)}$ and $\hat{\mathbf{T}}_{vw}^{(ij)}$ may be estimated from every baseline and the average $\bar{\mathbf{T}}_{gw}$ and $\bar{\mathbf{T}}_{vw}$ may be obtained. Finally, a vertical profile model may be employed to link the γ_{ij}^g and γ_{ij}^v between baselines and a unique solution may be obtained by minimizing the error of $\mathbf{\Pi}_{ij}$ in (10) for all baselines [3]. Finally, the original ground and volume components $\mathbf{T}_g^{ii}$ and $\mathbf{T}_v^{ii}$ may be obtained after de-whitening the estimated $\bar{\mathbf{T}}_{gw}$ and $\bar{\mathbf{T}}_{vw}$ with the corresponding $\mathbf{T}_{ii}$.
It is worth noticing that one of the key differences between the proposed ground and volume decomposition and the techniques based on the two largest Kronecker Product approximation [8] is that the proposed technique may be considered as a polarimetric decomposition in the sense that the equality in (7) *strictly* holds, instead of being just an approximation under some measure.

4 Results

To analyze the proposed technique, the TMPSAR08 L-band ESAR dataset will be employed. Two different multibaseline acquisitions of this dataset will be considered, consisting of 6 airborne acquisitions with similar baselines on each one, acquired on the 10th and 12th of June 2008 over the Traunstein site, in southern Germany. The main difference between these two images is that the acquisition on the 10th of June was performed after a large dry period (i.e. dry conditions) while the acquisition on the 12th of June was taken after a number of rain events occurring on the 11th and 12th of June (i.e. wet conditions). In this work the two datasets will be referred to as *dry* and *wet*, respectively. The Pauli RGB of the first image for the dry and wet acquisitions may be seen on Fig. 1a and 1d, respectively. Similarly, the Pauli RGB of the obtained covariance matrices $\mathbf{T}_g$ and $\mathbf{T}_v$ for the ground and volume are represented in Figs. 1b, 1e and 1c, 1f, respectively. The areas where the model could not be inverted are represented in black. They are mainly surface and bare areas where the two layer model do not apply.

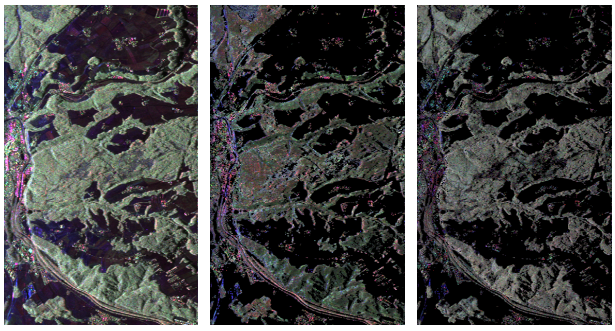

(a) Original - dry **(b)** Ground - dry **(c)** Volume - dry

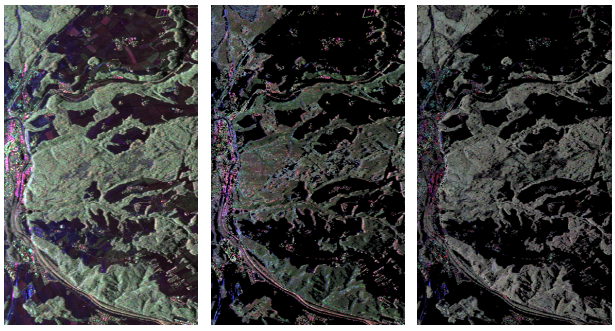

(d) Original - wet **(e)** Ground - wet **(f)** Volume - wet

Figure 1 Pauli RGB of the first acquisition and of the extracted ground and volume components for the dry and wet acquisitions.

In a first qualitative analysis of the data, no large differences may be observed. This is an expected results as the temporal baseline of only two days is not enough to produce significant changes over the vegetation. However, the change from dry to wet conditions may induce changes in the dielectric constant of the volume and ground layers. Indeed, a more closer look shows small differences between them. Fig. 2 shows the PDF over the image of the ground

to volume ratio for the dry and wet acquisitions, calculated as $\mathrm{tr}(\mathbf{T}_g)/\mathrm{tr}(\mathbf{T}_v)$. As it may be seen, on wet conditions smaller values of ground to volume ratios are obtained. This is consistent with the hypothesis of an increased reflectivity and extinction of the volume layer on wet conditions, predicted by some models. Moreover, it may be observed that the distribution is wider for dry conditions.

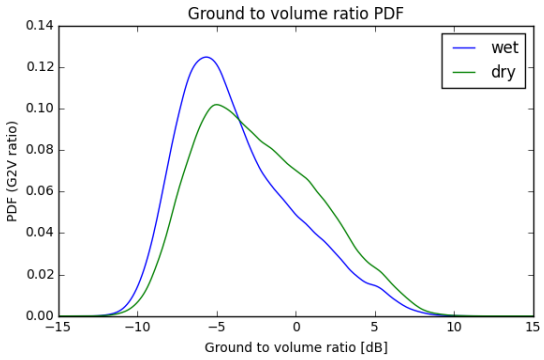

Figure 2 Histogram of the ground to volume ratio for the dry and wet acquisitions.

In order to analyze in more detail the change of power distributions between the two acquisitions, Fig. 3 shows the 2D scatter plot distribution between the dry and wet total power (the span) for the original data and for the extracted ground and volume components. It may be seen that on the original data, in Fig. 3a, most of the distribution is tightly concentrated around the diagonal, indicating no significant changes between both acquisitions. On the other hand, Figs. 3b and 3c show a wider distribution, presenting more values away of the diagonal. It may also be seen that on the ground component in Fig. 3b the distribution is slightly concentrated over the diagonal, while in Fig. 3c the opposite behavior is observed. This indicates that generally a small increase of the volume and a decrease of the ground component is observed on the wet acquisition, which may be consistent with the interpretation that on the wet acquisition more scattering and extinction is observed on the forest canopy.

However, the change in the components is not only visible in its power distribution but also on its polarimetry. For instance, Fig. 4 shows the scatter plot distribution of the Pauli1-Pauli2 phase of the extracted volume components for the dry and wet acquisitions. As it may be seen, there is a shift of the observed phase probably related to the change of dielectrics, having generally a larger Pauli1-Pauli2 phase for dry conditions.

In order to perform a more detailed analysis of the changes, the polarimetric change analysis technique proposed in [2][1] will be employed. Fig. 5 shows the obtained change representation for the increase and decrease in the original data and in the extracted ground and volume components. As it may be seen in Figs. 5a and 5b no significant changes may be observed on the original data, but the extracted ground and volume components, in Figs. 5c-5f, show a more defined change pattern, dominated by an increase of the ground and a decrease of the volume in dry

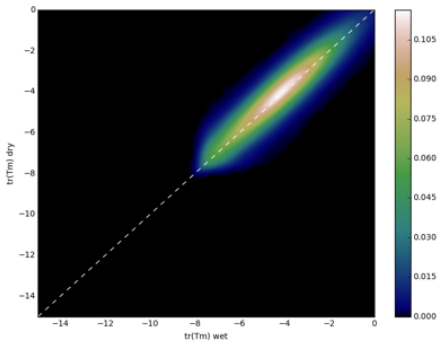

(a) Original dry vs. wet

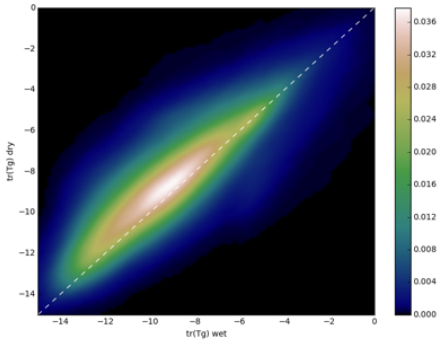

(b) Ground dry vs. wet

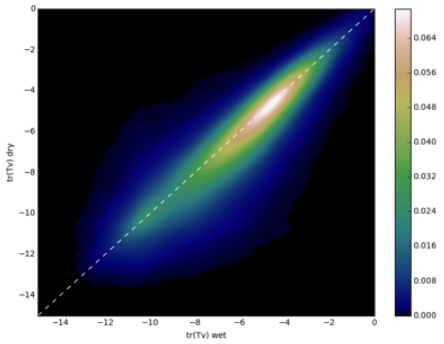

(c) Volume dry vs. wet

Figure 3 Scatter plot of the dry vs. wet total power (span) distribution for the (a) original, (b) ground and (c) volume components.

with respect to wet conditions.

This analysis shows that although the polarimetric change between the original dry and wet images is small, there is in fact a redistribution of the power within the ground and volume components, resulting in a larger change when analyzing these layers independently.

In order to see more clearly these redistribution of power, Fig. 6 shows the 2D distribution of the volume vs ground ratio changes, in dBs, between dry and wet conditions. This ratio is analyzed for each of the three Pauli components in Figs. 6a-6c, showing the volume ratio on the horizontal axis and the ground ratio on the vertical axis. The white dashed line depicts a inverse relation between them, for reference. In order to see the effect of the changes only over forested areas, a mask has been applied to consider only areas covered by trees with a height larger than 15

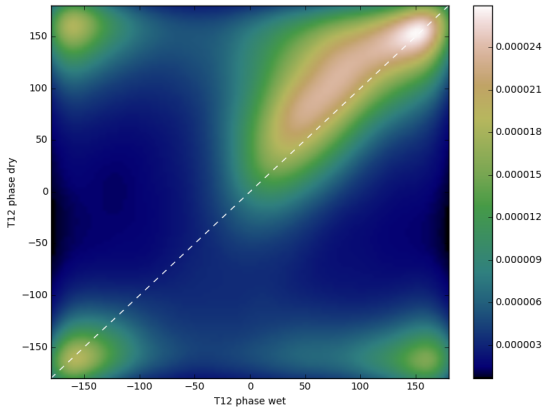

Figure 4 Scatter plot of the Pauli1-Pauli2 phase of the extracted volume components for dry and wet acquisitions.

meters, using a lidar acquisition as a reference.

In all the three plots of Fig. 6 it may be seen that the center of the distribution is located around 0 dB for the volume ratio but slightly higher, about 1 dB, for the ground ratio. This indicates a (small) general increase of the ground component on the dry acquisition, due to increased penetration. Although the distributions are generally centered, the inverse relation between them appears clearly on the plots. All three Pauli components follow an inverse relation, close to the white line, indicating that when the volume increases the ground decreases and vice-versa. It may also be seen that this relation is slightly more pronounced for Pauli1 and Pauli3 than for Pauli2, presenting a larger negative slope in Figs. 6a and 6c than in 6b.

In order to analyze the spatial distribution over the scene of the ground and volume ratios between dry and wet acquisitions, the following R_v and R_g ratios are defined

$$R_v = 10\log_{10}\frac{\text{tr}(\mathbf{T}_v^{dry})}{\text{tr}(\mathbf{T}_v^{wet})} \tag{14}$$

$$R_g = 10\log_{10}\frac{\text{tr}(\mathbf{T}_g^{dry})}{\text{tr}(\mathbf{T}_g^{wet})}. \tag{15}$$

Note that R_v and R_g correspond to the total power (the span) ratio between dry and wet acquisitions for the volume and ground components, respectively. With these quantities a ratio image may be composed with $|R_v + R_g|$, indicating with a high value where both increase or decrease, and $|R_v - R_g|$, presenting high values when they change in an opposite direction.

Fig. 7a shows this ratio image for all the invertible pixels of the image. Similar to a Pauli image, $|R_v + R_g|$ is represented in blue color while $|R_v - R_g|$ in the red channel. As a reference, Fig. 7b shows the forest height extracted from a lidar acquisition. It may be seen that over forested areas a red color is obtained while over areas with low vegetation the blue color dominates. This suggest that the ground scattering is also increasing due to the increase of water content and soil moisture but over forest the effect of increased extinction through canopy dominates, perceiving a general decrease over the ground component. This effect is more clearly visible on Fig. 7c, corresponding to the same image in Fig. 7a while masking areas with forest height below 15 meters. Comparing Figs. 7c and Fig. 7b it may be seen that there is some correlation between forest height and the amount of increase/decrease of the volume/ground components between dry and wet acquisitions. This reinforces the hypothesis that the decrease of power in the ground component is caused by the increase of extinction due to the wetter canopy, being in line with traditional vegetation scattering models.

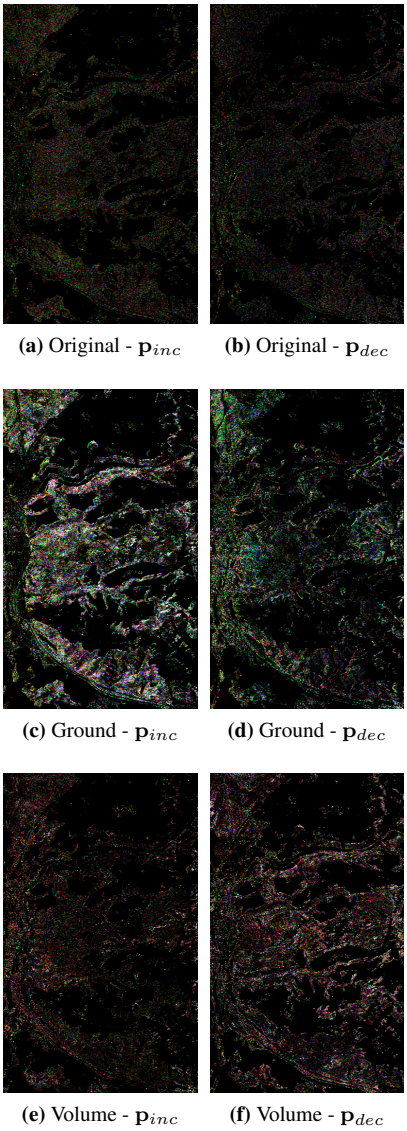

(a) Original - $\mathbf{p}_{inc}$ **(b)** Original - $\mathbf{p}_{dec}$

(c) Ground - $\mathbf{p}_{inc}$ **(d)** Ground - $\mathbf{p}_{dec}$

(e) Volume - $\mathbf{p}_{inc}$ **(f)** Volume - $\mathbf{p}_{dec}$

Figure 5 Polarimetric change representation of the increase and decrease ($\mathbf{p}_{inc}$ and $\mathbf{p}_{dec}$) between dry and wet datasets for the original data and the extracted ground and volume components. The change magnitude has been scaled from 1dB to 6dB.

5 Conclusions

This paper has employed a PolInSAR two layer model in order to perform a polarimetric decomposition of the ground and volume components over forested area. This

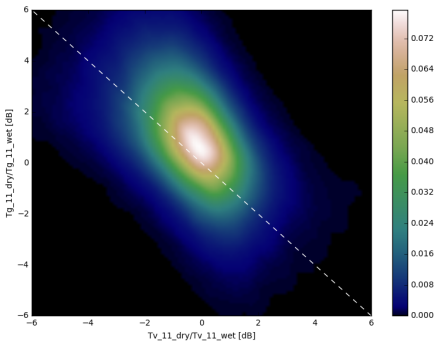

(a) Original dry vs. wet

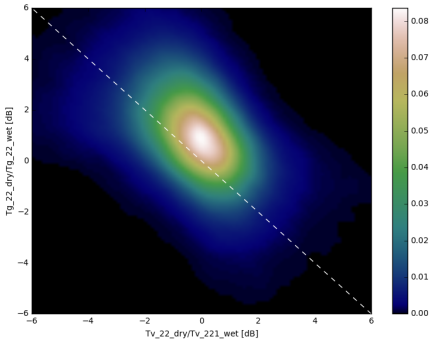

(b) Ground dry vs. wet

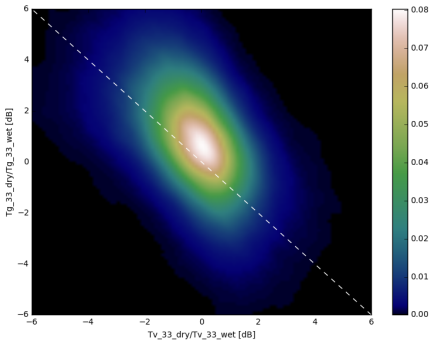

(c) Volume dry vs. wet

Figure 6 Power ratio changes in dB between dry and wet acquisitions for volume and ground components for (a) Pauli1, (b) Pauli2 and (c) Pauli3 polarization states. Areas covered by forest higher than 15 meters have been considered.

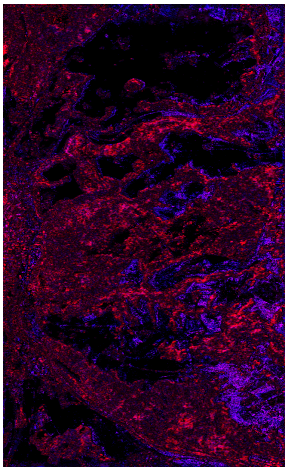

(a) Ratios image

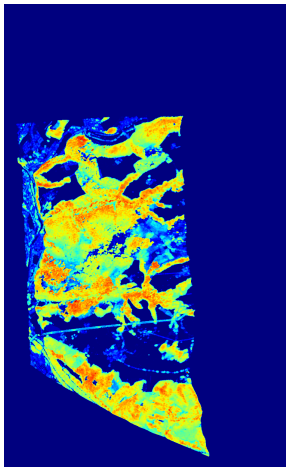

(b) Lidar forest height

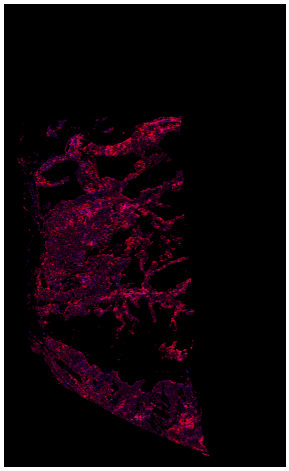

(c) Ratios image for height ≥ 15

Figure 7 Ground and volume ratio images and reference forest height. Ratio image for all the invertible pixels (a) and only for areas with forest height larger than 15 meters (c). In the ratio images $|R_v + R_g|$ is represented in blue (ground and volume change in the same direction) and $|R_v - R_g|$ is represented in red (ground and volume change in different direction). The intensity scaling of the ratio images is from 0 to 4dB. The reference lidar forest height is shown in (b) going from 0, in blue, to 50 meters, in red.

decomposition technique has been applied to compare two different multi-baseline acquisitions on distinct conditions over forest, one acquired after a dry period (dry) and the other after some rainy days (wet).

Although the polarimetric change between these dry and wet acquisitions was relatively small, it has been shown that the change on the individual ground and volume components was significantly larger. More specifically a redistribution of the scattering was observed. The increased water content on the forest canopy on the wet acquisition was translated into an increase of the volume scattering and extinction, resulting consequently into a decrease of the ground contribution. These observed changes are, therefore, in line with the expected response obtained from traditional physical scattering models. The performed experiments also show the potential of the proposed polarimetric ground and volume decomposition, based on the two layer PolInSAR model, to separate the different components within vegetation and to obtain more insight in the temporal changes occurring.

6 Literature

[1] A. Alonso-Gonzalez, T. Jagdhuber, and I. Hajnsek. Exploitation of agricultural polarimetric SAR time series with binary partition trees. In *POLINSAR 2015*, volume 729, 2015.

[2] A. Alonso-Gonzalez, C. Lopez-Martinez, K. P. Pa-

pathanassiou, and I. Hajnsek. Polarimetric SAR Time Series Change Analysis Over Agricultural Areas. *IEEE Transactions on Geoscience and Remote Sensing*, 58(10):7317–7330, 2020.

[3] A. Alonso-Gonzalez and K. P. Papathanassiou. Multibaseline Two Layer Model PolInSAR Ground and Volume Separation. In *EUSAR 2018; 12th European Conference on Synthetic Aperture Radar*, pages 1–5. VDE, 2018.

[4] J. Askne, P.B. Dammert, L.M. Ulander, and G. Smith. C-band repeat-pass interferometric SAR observations of the forest. *IEEE Transactions on Geoscience and Remote Sensing*, 35(1):25–35, 1997.

[5] S.R. Cloude and K.P. Papathanassiou. Three-stage inversion process for polarimetric SAR interferometry. *IEE Proceedings-Radar, Sonar and Navigation*, 150(3):125–134, 2003.

[6] Y. Cui, Y. Yamaguchi, H. Yamada, and S.-E. Park. PolInSAR Coherence Region Modeling and Inversion: The Best Normal Matrix Approximation Solution. *IEEE Transactions on Geoscience and Remote Sensing*, 53(2):1048–1060, 2015.

[7] C. Lopez-Martinez and A. Alonso-Gonzalez. Assessment and estimation of the RVoG model in polarimetric SAR interferometry. *IEEE transactions on geoscience and remote sensing*, 52(6):3091–3106, 2014.

[8] S. Tebaldini. Algebraic synthesis of forest scenarios from multibaseline PolInSAR data. *IEEE Transactions on Geoscience and Remote Sensing*, 47(12):4132–4142, 2009.